Proceedings of the International Gas Turbine Congress 2003 Tokyo
November 2-7, 2003

IGTC2003Tokyo TS-008

Numerical correction of pyrometry data from gas turbines

Jonas NICKEL[1], Helmut PUCHER[2] and Marco LÜDTKE[3]

[1]Department of Internal Combustion Engines
Technical University Berlin
Carnotstr. 1A, 10587 Berlin, GERMANY
Phone: +49-30-314-22607, FAX: +49-30-314-26105, E-mail: jonas.nickel@tu-berlin.de
[2]Technical University Berlin [3]Siemens Power Generation

ABSTRACT

This paper describes a new numerical tool for correcting measurement data from industrial gas turbine pyrometry systems developed by the department of Internal Combustion Engines of the Technical University Berlin in cooperation with Siemens Power Generation. Following a brief description of the basics of gas radiation the fundamental principles of the correction algorithms are explained. Subsequently, the program structure and its capabilities are described. Some examples and parametric discussions of the influence of gas turbine radiation on the pyrometry measurements are given as a demonstration. The paper concludes with some example calculations from a real gas turbine.

NOMENCLATURE

A	surface area
a	absorption coefficient
c	speed of light
c_2	second radiation constant
E	irradiancy
E_η	lower state energy
f	spectral distribution function
h	Planck's constant
k	Boltzmann's constant
L	steradiancy
N_A	Avogadro's number
n	coefficient of temperature dependence of γ_{air}
p	pressure
Q	total internal partition
$\dot{Q}$	heat transfer rate
$S_{\eta\eta\prime}$	spectral line intensity
T	temperature
γ	halfwidth at half maximum
δ	pressure shift
ε	emissivity
λ	wavelength
$\tilde{\nu}$	wavenumber
φ	irradiating number

Subscripts

air	air broadened
G	grey body
Gas	gas
i	incident
meas	measured
real	real value
ref	reference
refl	reflected
s	partial (pressure)
self	self broadened
η	lower energy state
$\eta\prime$	upper energy state

INTRODUCTION

Infrared turbine pyrometry has become a widely accepted and frequently applied tool in gas turbine development and monitoring. However, the ongoing efforts to improve the turbine efficiency lead to a number of problems that have to be overcome in order to achieve accurate temperature measurements of the turbine blades. Thermal barrier coated blades and compact annular combustion chambers installed close to the blades of the first turbine stage may cause a high level of infrared radiation noise which subsequently leads to increased uncertainty of measurement.

SOURCES OF RADIATION NOISE

The hot environment in a gas turbine yields several sources of infrared radiation. When measuring the radiation from a specific target - usually in order to determine its temperature - all other infrared radiation is considered to be noise which adversely affects measurement accuracy. Radiation noise can be split in two categories: direct and indirect noise. Direct noise is radiation emitted by a body or a gas. Examples for direct radiation sources are

- combustion chamber radiation,
- thermal radiation of the blades, the hub, and the casing,
- gas radiation.

Indirect noise is caused by reflection of infrared radiation from a surface like the blades or the turbine casing.

Manuscript Received on April 2 ,2003

Naturally, both types can occur simultaneously on the same surface (e.g. the turbine blades). The distinction, however, is important since the emission process determines the spectral distribution of the radiation. Depending on the spectral sensitivity of the detector used for the measurement some sources can be ignored. In the following sections the most important sources of radiation noise are described in detail.

Radiation from the Combustion Chamber

The combustion chamber of a gas turbine is not only the source of the hot working gas for the turbine but also a major source of infrared radiation. Depending on the engine design the chamber is more or less visible from the turbine blades. In modern gas turbines with annular combustion chambers the combustion chamber outlet is directly connected to the turbine which also means that a considerable amount of infrared radiation is emitted towards the turbine. The degree to which this causes radiation noise depends on several factors. The first and most important factor is the fuel used in the turbine as it strongly influences the flame radiation in the combustion chamber. While combustion chambers running on natural gas emit only relatively low levels of flame radiation turbines running on oil do emit very high levels of flame radiation. This can be compared to the visible part of the spectrum where natural gas flames are almost invisible while oil flames emit a bright yellow light. The effect of flame radiation is particularly strong in the near infrared because the combustion chamber behaves similarly to a grey body. The second most important factor influencing the radiation noise is the reflectivity of the turbine material. As long as casing, hub and turbine blades consist of conventional heat resistant alloys the overall reflectivity is relatively low leading only to a small influence of combustion chamber radiation. Thermal barrier coatings which are now frequently applied to several turbine components have a high reflectivity causing a considerably higher influence of combustion chamber radiation. Under unfavourable conditions reflected flame radiation can reach up to 70% of the temperature measurement signal on the first turbine stator blade row (Suarez, 1994).

Thermal Barrier Coated Blades

In recent years Thermal Barrier Coatings (TBC) are increasingly used for turbine blade insulation in order to achieve higher turbine inlet temperatures. While these materials have many advantages their emission characteristics are quite unfavourable for infrared temperature measurements. TBC materials like Zirconia have very low emissivities in the near infrared (see Fig. 1), combined with some transparency that depends on the coating thickness. Furthermore, the emissivity changes over time due to deposits and ageing of the material. Unfortunately, many high-speed pyrometry systems use silicon photo diodes, which have their peak sensitivity in the 1 μm range. Hence, accurate measurements are extremely difficult to achieve when using a 1 micron pyrometer on gas turbines with TBC blades.

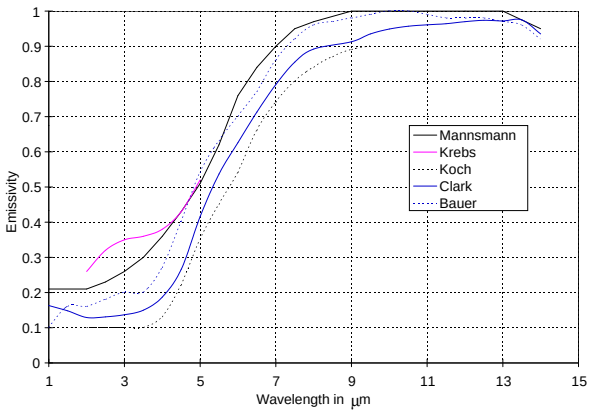

Fig.1: Emissivity of Zirconia

A solution to the problem is to measure the temperature in the thermal infrared around 10 μm where most TBC materials have a high emissivity. Suitable for that purpose are pyrometer systems which operate in the 10 μm range using e.g. a HgCdTe-detector. Even though many problems can be solved with this approach there are still a number of factors that have to be considered when measuring in this band. The effects of the deposits on the emissivity in the 10 μm range have to be known. Furthermore, water vapour and carbon dioxide are not diathermal in this band but do emit a considerable amount of radiation which has to be compensated for. Finally the flame radiation is more dominant in the thermal infrared.

Infrared Gas Radiation

The working gas entering an industrial gas turbine consists approximately of 5 percent carbon dioxide and 10 percent water vapour. While these two compounds are almost diathermal in the near infrared around 1 μm their emissivities cannot be ignored for higher wavelengths. Therefore, when measuring the temperatures on TBC blades with an infrared pyrometer a suitable spectral window with relatively low gas emissivities has to be chosen first. A good choice is usually the range between 9 and 14 μm in the thermal infrared, which is a well known spectral window for atmospheric observations. However, under the conditions found in a gas turbine water vapour as well as carbon dioxide emit some gas radiation that has to be analytically removed from the measurement signal in order to obtain sufficiently accurate results.

CORRECTION OF GAS RADIATION

While solid bodies emit continuous spectra, which often resemble that of grey radiators, gases emit radiation in a number of specific bands. These emission bands consist of a number of spectral lines. The emission mechanism of gases is the transition between different discrete vibrational and rotational states of the gas molecules. The number and intensity of spectral lines depends on the number of possible oscillation states in a gas molecule and transition probability between them. In general, it can be said that the number of oscillation

states increases with the complexity and asymmetry of a molecule. For example, symmetrical, two-atomic molecules exhibit only a fraction of the number of spectral lines observed on more complex molecules. Hence, gases like oxygen and nitrogen hardly emit any infrared radiation and are considered to be transparent in the infrared. Gases like water vapour and carbon dioxide on the other hand develop a vast number of oscillational states causing a considerable amount of infrared radiation. When evaluating measurements from gas turbines this radiation will have to be taken into account.

Based on the knowledge of the spectral distribution of the gas emissions appropriate measuring windows with relatively low gas emissivities can be found. Yet for the turbine pyrometry in the thermal infrared a small portion of gas radiation always remains. In order to achieve good measurement accuracy this radiation noise will have to be removed from the measured data. This can be done either by differential pyrometry (Suarez, 1994) or by numerical correction, which will be considered here. The numerical correction requires a detailed knowledge of the emission characteristics of the combustion gas. Simplified emission spectra have been previously used in order to estimate the amount of gas radiation noise and the measurement error introduced by it (Gröber, 1988). For an accurate correction it is necessary to use a database containing detailed information about the spectral lines of each individual species. One of the most complete databases is HITRAN, developed by the Air Force Cambridge Research Laboratories and maintained by Harvard-Smithsonian Center for Astrophysics. It contains more than 1,080,000 spectral lines for 36 different molecules. However, as HITRAN is a database used in atmospheric spectroscopy it is compiled for a temperature of 296 K and a pressure of 1000 hPa. Even though the intensities of the spectral lines can be converted to other gas states in the way described below the operating conditions in a gas turbine are too different from atmospheric conditions to do the conversion with a high confidence. Instead, it is advisable to use the database HITEMP which is the high temperature version of HITRAN. It consists of the spectral datasets for water vapour and carbon dioxide for a base temperature of 1000 K at 1000 hPa. The higher base temperature helps to minimise possible extrapolation errors. However, since the line intensities have to be calculated for a considerably extrapolated pressure range as well as some uncertainties regarding the accuracy of the line intensities remain. The following paragraphs describe the algorithms required for the correction of temperatures measured in the presence of infrared gas radiation.

In order to be able to compensate the deviations caused by non-diathermal gas an equivalent emissivity has to be defined. Using this emissivity the corrected temperature can be determined. For illustration purposes the signal detected by a pyrometer sensor shall be considered. This signal is proportional to the irradiancy E. When the geometry of the light path is known (which is usually the case) the steradiancy L can be calculated and used for all subsequent calculations. The steradiancy of a grey body in the wave number range between $\tilde{\nu}_1$ and $\tilde{\nu}_2$ is given by the equation

$$L_{G,\tilde{\nu}_1-\tilde{\nu}_2} = \int_{\tilde{\nu}_1}^{\tilde{\nu}_2} \varepsilon 2hc^2\tilde{\nu}^3 \frac{1}{e^{\frac{hc\tilde{\nu}}{kT}}-1} d\tilde{\nu}. \qquad (1)$$

In turbine pyrometry the observed surface is usually assumed to be a grey body surface thus allowing to determine the measured temperature T_{meas} using Eq.(1). However, in the presence of gas radiation this measured temperature does not represent the real surface temperature T_{real} since the hot gas absorbs a part of the surface radiation while adding its own radiation to the infrared signal. For a hot gas layer of thickness X this process is described by the equation

$$\begin{aligned} L_{G_{meas},\tilde{\nu}_1-\tilde{\nu}_2} = \int_{\tilde{\nu}_1}^{\tilde{\nu}_2} & \left(1-e^{-a_{\tilde{\nu}}X}\right)\varepsilon L_{G_{real},\tilde{\nu}} \\ & + L_{Gas,\tilde{\nu}} e^{-a_{\tilde{\nu}}X} d\tilde{\nu}, \end{aligned} \qquad (2)$$

which can be used to determine the real surface temperature. The value $a_{\tilde{\nu}}$ in Eq.(2) is called the spectral absorption coefficient of the hot gas. Depending on the composition of the gas it can either be calculated using the absorption characteristics of one sort of molecules or of a mixture of molecule species. In the latter case the spectral absorption coefficient is determined by adding the spectral absorption coefficients of the individual species. The absorption coefficient for one sort of molecules is found by evaluating the data of all spectral lines of this molecule at the wave number range under consideration.

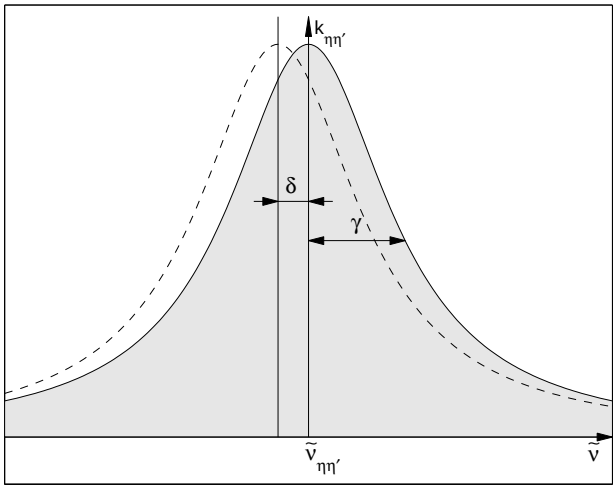

Fig.2: Structure of a spectral line

The structure of a single spectral line is shown in Fig. 2. The centre of the line for the transition between the states η and $\eta\prime$ lies at the transition wave number $\tilde{\nu}_{\eta\eta\prime}$. Under atmospheric conditions as well as conditions of higher pressure or temperature the spectral line is

not infinitely small. Instead, the intensity is distributed according to a Lorentz profile:

$$f = \frac{1}{\pi} \frac{\gamma(p,T)}{\gamma(p,T)^2 + \left[\tilde{\nu} - (\tilde{\nu}_{\eta\eta'} - \delta(p_{ref})p)\right]^2}. \quad (3)$$

The parameter γ is called the halfwidth at half maximum of the spectral line. Its value depends on several line broadening mechanisms, e.g. natural line broadening, collision broadening, and Doppler broadening. A consolidated equation for the calculation of γ is given by

$$\gamma(p,T) = \left(\frac{T_{ref}}{T}\right)^n (\gamma_{air}(p_{ref},T_{ref})(p-p_s) + \gamma_{self}(p_{ref},T_{ref})p_s), \quad (4)$$

where γ_{air}, γ_{self}, and n are transition dependent and have to be supplied by a database.

The value δ is the air-broadened pressure shift, given at reference conditions. Since this value is almost always zero for the spectral lines of the gases under consideration in this paper, a detailed discussion of δ is omitted here. The grey area under the curve in Fig. 2 is equivalent to the spectral line intensity $S_{\eta\eta'}$. In databases the spectral line intensity is usually given for a reference temperature T_{ref}. Using the equation

$$S_{\eta\eta'}(T) = S_{\eta\eta'}(T_{ref}) \frac{Q(T_{ref})}{Q(T)} \frac{e^{\frac{-c_2 E_\eta}{T}} \left(1 - e^{\frac{-c_2 \tilde{\nu}_{\eta\eta'}}{T}}\right)}{e^{\frac{-c_2 E_\eta}{T_{ref}}} \left(1 - e^{\frac{-c_2 \tilde{\nu}_{\eta\eta'}}{T_{ref}}}\right)} \quad (5)$$

the spectral line intensity can be converted to other temperatures. The total internal partition sums Q(T) are usually interpolated from an accurate evaluation of the partition function while the lower state energy E_η is part of the measured data supplied with spectral databases.

Multiplying the spectral line intensity with the corresponding spectral profile yields the monochromatic absorption coefficient $k_{\tilde{\nu}_{\eta\eta'}}$:

$$k_{\tilde{\nu}_{\eta\eta'}} = S_{\eta\eta'}(T) f. \quad (6)$$

Now, the spectral absorption coefficient can be calculated:

$$a_{\tilde{\nu}} = k_{\tilde{\nu}_{\eta\eta'}} \frac{p_s N_A}{RT}. \quad (7)$$

For each wave number all spectral lines that spread into this wave number range have to be evaluated and the resulting spectral absorption coefficients have to be added up. It is important to note that according to Eq.(3) the spectral lines would be spread across the whole spectrum. Hence, all spectral lines of the molecules under consideration would have to be evaluated for each wave number. Since the spectra of technically important molecules consist of several thousand spectral lines such an evaluation is deemed impractical. In order to save computation time a sensible cut-off intensity has to be chosen.

Finally, the spectral absorption coefficients gained with the equations described above can be used to calculate the effect of gas absorption and gas radiation on the measured signal, which can then be corrected.

CORRECTION OF COMBUSTION CHAMBER RADIATION AND REFLECTED RADIATION

As already stated in the introduction, the flame radiation and its reflection can be a considerable source of radiation noise in the near infrared when turbine components such as the turbine blades or the hub are coated with a ceramic thermal barrier. The high reflectivity of TBC materials caused by their low emissivity leads to a superposition of a relatively weak temperature signal with a rather strong reflection signal. This situation becomes even more complicated for modern gas turbine designs where the distance between the first turbine stator blade row and the annular combustion chamber is small. In these engines a high level of direct and indirect flame radiation can be expected on the first stator blades as well as on parts of the first rotor blades. For the numerical model described in this paper, only indirect flame radiation is considered due to the instationary characteristics of flames. Furthermore, most combustion chambers form a cross-sectional cavity in which a significant part of the emitted radiation is reflected several times before it is emitted into the turbine. Hence, a simplification is possible which assumes the combustion chamber to be a black body radiator with an opening identical to the combustion chamber outlet. This assumption is kept in the following discussions. However, the algorithms described below are generally applicable and could be adapted to suit other radiation distributions as well as other geometric designs of the combustion chamber.

The reflected radiation superimposing the actual temperature signal from the blades consists of the radiation from the combustion chamber, the radiation emitted by neighbouring blades as well as other components of the turbine, and the radiation reflected by those turbine components. The following sections describe the model used for the reflection calculations and three possible algorithms to calculate the radiation flux in the turbine.

Radiative Transfer

Calculating the radiation flux through the first stages of an industrial gas turbine is a complex task, especially if the demands for calculation accuracy are high. In difference to the many well known raytracing and shading algorithms used in computer graphics, it is not satisfactory if something *looks* right. Instead, the computed data have to be *physically* correct. Hence, the common simplifications used in these algorithms are not applicable radiative transfer calculations. The algorithms described here are kept as general as possible

in regard to the geometric setup of the engine. The radiation emission, however, is only calculated for the full spectrum of black body radiators in order to reduce computation time. Yet a modification to accommodate for other spectra could relatively easily implemented.

The radiative heat transfer rate between two surfaces A_1 and A_2 is given by the equation

$$\dot{Q}_{12} = \frac{\sigma\varepsilon_1\varepsilon_2 A_1\varphi_{12}}{1-(1-\varepsilon_1)(1-\varepsilon_2)\varphi_{12}\varphi_{21}}\left(T_1^4 - T_2^4\right), \qquad (8)$$

where φ_{12} and φ_{21} are called irradiating numbers and are defined by

$$\begin{aligned}\varphi_{12} &= \frac{1}{\pi A_1}\int_{A_1}\int_{A_2}\frac{cos\beta_1 cos\beta_2}{R^2}dA_2\,dA_1 \quad and\\ \varphi_{21} &= \frac{A_1}{A_2}\varphi_{12}.\end{aligned} \qquad (9)$$

Radiation Reflection

Reflection phenomena can be roughly divided in specular, directional diffuse, and uniform diffuse reflection. The reflection characteristics of a surface can be described by its bidirectional reflectance distribution function. However, for the surfaces found in an industrial gas turbine these functions are usually not readily available. Yet, since the components used in a turbine have a rather rough surface structure the assumption of a uniform diffuse reflection is considered to be acceptable.

When a surface with a given emissivity ε reflects an incident radiation with the steradiancy L_i the reflected heat flux can be described by the equation

$$\dot{Q}_{refl} = \varphi_{12}\pi A_1 L_i(1-\varepsilon). \qquad (10)$$

The superimposition of radiation from several sources leads to a linear addition of all heat fluxes and steradiancies. For the calculation of the radiation apparently emitted by a surface element, all reflected heat fluxes have to summed up and added to the heat flux actually emitted by the surface. Then, this heat flux can be converted back into a steradiancy or a virtual temperature using e.g. a grey body radiation model. The steradiancy coming from a surface can subsequently be used to follow the path of the radiation through the turbine as described in the section below.

Correction Algorithms

The correction algorithms described in this section have been developed with regard to a universal application to many possible geometries. Consequently, very few assumptions have been made in respect to the properties of the objects used in the geometrical model. No other primitives than triangles and rectangles are used due to the fact that the geometries in a gas turbine cannot be explicitly described by simple geometric bodies and that arbitrary temperature profiles should be applicable to all surfaces. Furthermore, techniques like backface culling can be used to reduce computation time. The discretisation for a typical stator blade is shown in left half of Fig. 3

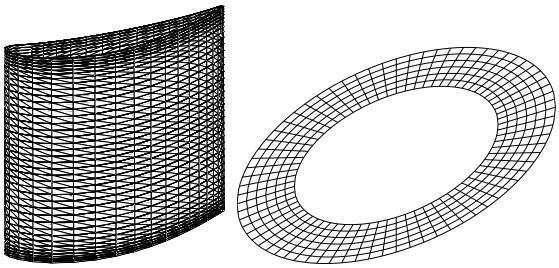

Fig.3: Discretisation of the Combustion Chamber and a Stator Blade

In total, three algorithms have been developed along different ideas for the calculation of the radiation propagation. The algorithms were then studied in regard to their required computation time for a given accuracy and to their sensitivity to the discretisation of the model.

All radiation sources including the reflecting surfaces are assumed to be uniform diffuse radiators. The radiation propagation is calculated for the whole spectrum and any gas radiation is ignored. The combustion chamber is treated as a black body radiator while the blades, casing, hub and pyrometer probes are treated as grey body radiators.

A Simple Raycasting Algorithm. The first and simplest algorithm calculates the propagation of radiation emitted by the combustion chamber. The combustion chamber is discretised into a number of concentric rings, which are subsequently divided into segments (see Fig. 3, right). Then the hemisphere above each segment is split into small sections, with each of them assigned with the corresponding portion of the radiation emitted by the combustion chamber segment. Subsequently, the intersections between the axis of each section and the turbine components is calculated. The radiation portion of the section is then assigned to the element closest to the combustion chamber. This process is repeated for all sections of all hemispheres of all combustion chamber segments.

Although this algorithm was very helpful during the first development phase of the correction program it proved to be very computing time consuming. Furthermore, the calculation of secondary reflections could not be handled with a reasonable amount of work. This lead to the creation of an improved algorithm for the calculation of the radiation propagation.

An Improved Raycasting Algorithm. The improved raycasting algorithm also starts with a segmented combustion chamber, but instead of simply trying to find elements, which are hit by fixed rays of radiation emitted from each segment the light

paths between the combustion chamber segments and the turbine elements are directly calculated. The algorithm then has to find out which turbine elements block the views of others. This is done by a combination of Z-buffering and a comparison of the lights paths' directions. Once all visible light paths have been established the radiation transfer between the combustion chamber segments and the elements corresponding to the lights paths is calculated using Eq.(8).

All subsequent reflections as well as radiation transfer between the components of the turbine can be computed by the same algorithm. If the algorithm is used in the way just described it calculates the amount of radiation superimposed on the radiation naturally emitted by the surfaces of the turbine components. This means using the real temperatures in the gas turbine the algorithm calculates the virtual temperatures measured by a pyrometry system. If the temperatures measured with a pyrometer instead of the real temperatures are known the algorithm can be either iteratively used to establish the real temperatures or the calculation principles can be inverted to directly calculate the real temperatures. Depending on the relation of the amount of real temperatures (measured e.g. with thermocouples) to the amount of temperatures gained with a pyrometry system one of both calculation direction will be more feasible.

A Raytracing Algorithm. A previous work (Salden, 1990) used a kind of raytracing algorithm to calculate the radiative transfer between the combustion chamber and the other turbine components. For comparison reasons a similar raytracing algorithm was implemented. Instead of starting from the combustion chamber the raytracing algorithm begins with the elements that make up the turbine components. For each element a list of visible turbine elements is created and if radiation is present on one of the elements the radiation transfer is calculated. Otherwise the ray is traced back a predetermined number of reflections until it either reaches the combustion chamber or is regarded as not transferring any radiation. Similar to the improved raycasting algorithm the raytracing also allows several reflections as well natural radiation emission on all components in the turbine. Both algorithms are compared in the results section.

RESULTS

The algorithm dealing with gas radiation and the one calculating the combustion chamber radiation are not used in conjunction. There are two reasons for this: firstly, the gas radiation is more dominant in the thermal infrared while the reflection phenomena are more critical in the near infrared, where TBC materials have a low emissivity. Secondly, combining both algorithms for a single calculation would lead to a significant increase in computation time that could currently not be justified by the improved accuracy. Therefore, computation results are presented separately for the gas radiation and the radiation reflection.

Gas Radiation

The effect of gas radiation on pyrometry measurements depends on the assumptions made for the measurements as well as on boundary conditions present in the measured system. Two examples given below discuss the influence of some chosen parameters. In both examples the following boundary conditions are kept constant:

- total gas pressure = 16 bar,
- partial pressure of water vapour = 1.6,
- partial pressure of carbon dioxide = 0.7,
- observation wavelengths = 9 - 11 m.

Fig. 4 shows the effect of surface emissivity and the thickness of the gas layer between the surface and the pyrometer system on the measurements. It is assumed that the pyrometer system delivers a target temperature of 1300 K under black body radiator conditions. The graph then shows the real temperature creating the corresponding signal for a number of surface emissivities and gas layer thicknesses. The fact that the real temperature decreases with increasing gas layer thickness for a given emissivity shows that the gas emits more radiation than it absorbs for the conditions considered here. Furthermore, it can be seen that the real temperature increases with decreasing emissivity which means the surface temperature can be underestimated if the surface emissivity is overestimated. The interesting aspect about this rather well known fact is that it compensates for the higher emissivity of the gas leading to a (gas layer thickness and emissivity) range where the measured and the real temperature are equal. In the diagram the break-even is visible as a horizontal line at 1300 K.

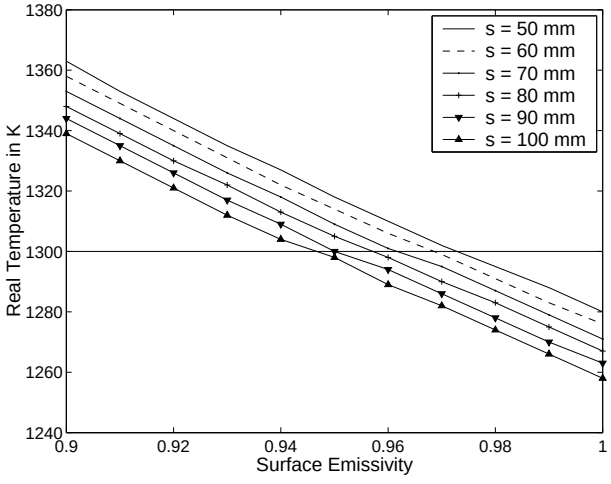

Fig.4: Real Temperature versus emissivity

In Fig. 5 the dependency of the real (component) temperature on the gas temperature can be seen for several measured temperatures. The gas layer thickness is set to 100 mm and the surface emissivity is set to one. While measured and real temperature are equal if the temperature of the gas layers agrees with the measured temperature, the real temperature decreases rapidly with

increasing gas temperature. A gas layer which is about 200 K warmer than the measured temperature, will yield a difference of 30 K between the measured and the real temperature.

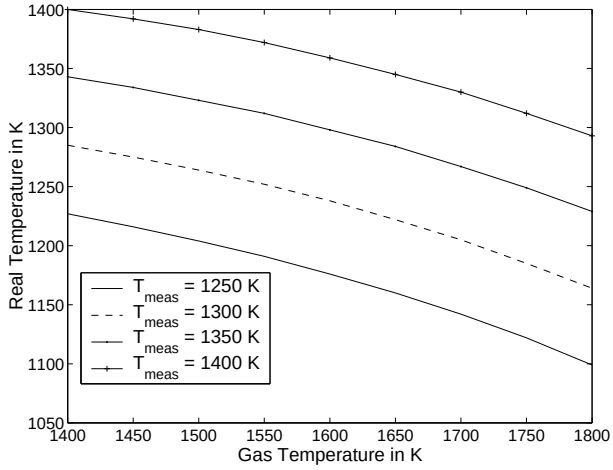

Fig.5: Corrected temperature versus gas temperature

Radiation reflection

The ratio between the emitted and the reflected radiation depends strongly on the emissivity of the surface and the level of the ambient radiation. Fig. 6 shows the variation of the measured temperature with the emissivity of the surface and the level of ambient radiation (T_{amb} is the equivalent black body temperature of the ambient radiation). It can be seen that the measured temperature increases rapidly with decreasing emissivity. It is important to note that interpreting the surface radiation as a black body radiation rather than using the true emissivity dampens the temperature increase. The reason is that the reflected ambient radiation which contributes significantly to the measured radiation level has to be interpreted as a higher surface temperature. A lower emissivity would thus yield far higher measured temperatures. This discussion again shows the significance of a correction algorithm.

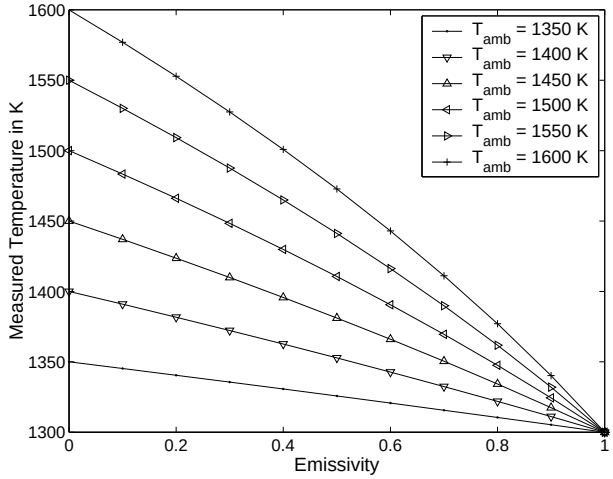

Fig.6: Influence of emissivity and ambient radiation on the measured temperature

Accuracy of Computation.

In difference to the correction of gas radiation the algorithm for the correction of reflected radiation needs a suitable geometrical model which has to be tested prior to an integrated model with measured data. Three computation algorithms have been described earlier in this paper. In order to find the best one a test case with an existing analytical solution has been calculated using the improved raycasting and the raytracing algorithm. The accuracy of computation for a given discretisation and the required discretisations for a given accuracy have been determined. The test case is shown in Fig. 7. It shows a surface element ΔA_1 which is positioned along the coaxial normal of a circle A_2. The element is rotated by the angle β and the circle is seen from element under the angle 2α.

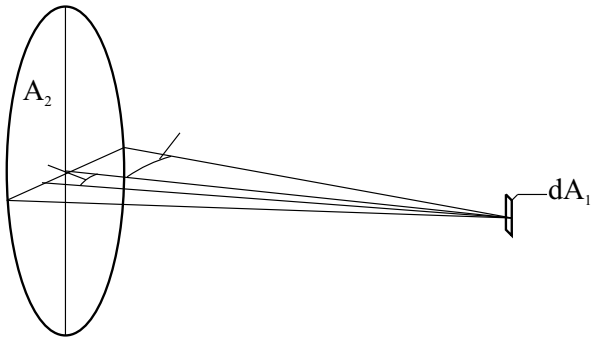

Fig.7: One of the test cases used for algorithm evaluation

The analytical solution for this case (see (VDI, 1997)) is given by the equation

$$\begin{aligned} \varphi_{12} &= \sin^2\alpha\cos\beta \quad for(\alpha+\beta) \le 90°, \\ \varphi_{12} &= \frac{\alpha - \sin\alpha\cos\alpha}{\pi} for\beta = 90°. \end{aligned} \tag{11}$$

With these irradiating numbers the reflection process can be calculated. For the verification a circle with a diameter of 100 mm and a surface element at the distance 50 mm and the rotation 30° shall be considered. The relation of circle diameter and distance yields an observation angle of $\alpha = 45°$. For these values irradiating number is $\sqrt{3}/4 \approx 0.43301$. The numerical calculations are run with several discretisations of the circle which is split into a number of concentric rings which are then split into the same number of segments. The comparison of the raycasting with the raytracing algorithm shows that the raycasting algorithm converges very quickly. A combustion chamber discretisation of eight rings each divided into eight segments is sufficient to achieve an irradiating number of 0.4315, which is considered to be convergence. The raytracing algorithm, however, requires a 32 x 32 discretisation to achieve a similar result.

Computation speed.

The results described above mean that a calculation using the raycasting algorithm is sixteen times faster than a calculation using the raytracing algorithm, if

both algorithms have the same iteration speed. In order to evaluate this the example described above has been given to both algorithms using the same discretisation. The raycasting calculation took 83 s while the raytracing calculation took some 1410 s. Hence the raycasting algorithm is 270 times faster than the raytracing algorithm in its current state. A closer investigation also revealed that in difference to the raycasting the computing time of the raytracing increases with the square of the number of elements instead of increasing linearly. Although there is some potential to optimise the raytracing algorithm it is not very likely that it will reach the speed of the raycasting algorithm. Therefore, the raycasting algorithm is currently preferred for further development.

DATA FROM A REAL GAS TURBINE

The effect of combustion chamber radiation on the stator blades of a heavy duty gas turbine have been studied in detail using a numerical model of a Siemens V84.3A(2). A realistic surface temperature profile for the first stage stator blades was calculated and the effect of combustion chamber radiation on the measured profile was computed. The result is shown in Fig. 8.

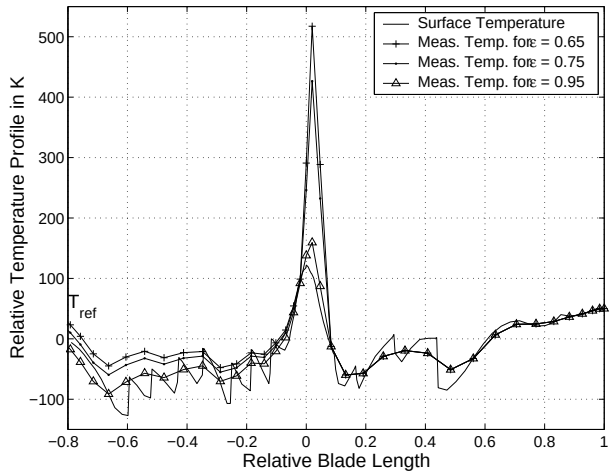

Fig.8: Comparison of the surface temperature versus several measured temperature profiles for a first stage stator blade

The figure shows the circumferential temperature profile at the mean diameter of the blade. T_{ref} denotes the reference temperature for the shifted temperature profiles. The temperature at the leading edge of the blade can be seen in the middle of the graph. The left hand side of the figure represents the pressure side of the blade while the right hand side shows the suction side of the blade. It can be seen that the flame radiation significantly raises the measured temperature at the leading edge and the pressure side of the blade. This effect increases dramatically with decreasing blade emissivity. For a blade emissivity of $\varepsilon = 0.95$ the original profile is still well recognisable, and the maximum temperature difference approaches about 50 K. For lower emissivities, however, the flame radiation becomes increasingly dominant making it more difficult to extract the original temperature profile. Considering the additional noise present in a heavy duty gas turbine it becomes clear that although a correction of the measured data might be possible for emissivities lower than 0.65 it does not appear to be practical. Furthermore, it has to be noted that the considerations presented here apply only to the full radiation spectrum. Depending on the wavelength of the peak sensitivity of the measurement system in use the impact of flame radiation on the measurements can vary considerably.

CONCLUSIONS

In this paper the problems for infrared pyrometry on modern heavy duty gas turbines have been described. Using approaches found in astrophysics and radiative heat transfer a new numerical tool has been developed. This tool calculates the gas radiation as well as the flame radiation present in an industrial gas turbine. Each radiation sources can then be used to predict the expected deviations of the measured values and to correct the pyrometry measurements. The effects of both radiation sources on the measurements have been shown by some examples and the possibilities and limitations of numerical data correction have been pointed out. A future development might include features like a simultaneous consideration of both radiation sources for correction or the simulation of multi-spectral pyrometry.

References

Markham et al., 2001, "Simultaneous Short and Long Wavelength Infrared Pyrometer Measurements in a Heavy Duty Gas Turbine," Proceedings, ASME Turbo Expo 2001, New Orleans, LA.

Gröber, Erk, Grigull, 1988, "Die Grundgesetze der Wärmeübertragung," Springer, Berlin, Heidelberg, p. 395.

Penner, S. S., 1959, "Quantitative Molecular Spectroscopy and Gas Emissivities," Addison-Wesley, Reading, MA, pp. 1-37 .

Rothman et al., 1998, "The HITRAN Molecular Spectroscopic Database and HAWKS (HITRAN Atmospheric Workstation): 1996 Edition", Journal of Quantitative Spectroscopy and Radiative Transfer, Vol. 60, pp. 665-710.

Salden, D., 1990, "Ein Beitrag zur Optimierung der Auslegung und Kalibrierung sowie zur Diskussion der Messgenauigkeit eines berührungslos arbeitenden Oberflächentemperaturmessverfahrens im Hinblick auf einen Einsatz an schnell rotierenden Laufgittern von Kleingasturbinen," Ph.D. Thesis, RWTH Aachen, Germany.

Suarez, E., 1994, "Temperature Measurements of Thermal Barrier Coated Turbine Blades", Proceedings of the NASA Remote Temperature Sensing Workshop, NASA Lewis Research Center, NASA Conference Publication 10167, (Oct. 27 - 28, 1994).

VDI, 1997, "VDI-Wärmeatlas," 8th Ed., Springer, Berlin, Heidelberg, pp. Ka 1 - Kb 10.